Acoustic Emission (AE) source localization using Extended Kalman Filter (EKF)

Ehsan Dehghan Niri*[a], Salvatore Salamone[a], Puneet Singla[b]
[a]Smart Structures and Research Laboratory,112 Ketter Hall, Civil Structural and Environmental Engineering Department, State University of New York at Buffalo (UB), NY, USA 14260;
[b] Mechanical and Aerospace Department, State University of New York at Buffalo (UB), NY, USA 14260;

ABSTRACT

This paper presents a method for Acoustic Emission (AE) source localization in isotropic plate-like structures based on the Extended Kalman Filter (EKF). The accuracy of the traditional triangulation methods depends on the time of flight (TOF) measurements and on the group velocity assumption so uncertainties in both should be taken into account and filtered out. An algorithm based on the Extended Kalman Filter (EKF), capable of filtering out these uncertainties, has been developed for the estimation: 1) the AE source location and 2) the wave velocity. Experimental tests have been carried out on an aluminum plate to show accuracy and robustness of the proposed approach.

Keywords: Acoustic Emission (AE), Triangulation, Time of Flight (TOF), Lamb wave, Extended Kalman Filter (EKF)

1. INTRODUCTION

In the past two decades, significant efforts have been made towards the development of integrated structural health monitoring (SHM) systems in order to increase safety of aircraft systems and reduce life cycle costs[1]. Damage location using Lamb waves in plate like structures, can be achieved under either an "active" or a "passive" mode. Under the "active" mode, diffractions of piezoelectrically-actuated waves can be used to locate existing damage in a post-mortem mode[2,3]. Under the "passive" mode, growing damage (e.g. fatigue cracks), or sudden impacts can be located by monitoring acoustic emissions in a real-time mode[4,5,6,7,8]. This paper focuses on the "passive" monitoring technique using a sparse array of piezoelectric transducers to locate the point of AE source. Traditionally, damage or impact location is based on time-of-flight (TOF) triangulation of wave measurements taken at multiple receiving points. This technique works very well when the wave velocity (V_g) in the test material and the arrival time (t_i) of the signal at all three sensor locations are known. The damage or impact location is identified by drawing three circles of radii (R_i), whose centers coincide with the three sensor locations. The radius R_i is obtained by multiplying the time of arrival of the signal (t_i) with the wave velocity (V_g). The intersection point of these three circles is the damage location (figure 1). However, the exact time of arrival of the signal may not be known either because of the distortion of the signal due to dispersion phenomena or because the instrument noise hiding the exact time of arrival of the signal[4]. In addition, environmental interference, such as temperature changes, significantly affects the TOF measurements of acoustic waves and wave velocity[9]. As a result, rather than the damage being located at a single point at the intersection of the circles, the damage can be located anywhere in the dark overlapped region at the intersection of the rings around the sensors locations (figure 1). The ring's width represents the uncertainty in the measured distance as a result of TOF and/or wave velocity uncertainties. In general, the lower the signal-to-noise ratio (SNR) the higher is the ring's width (i.e. higher

* ehsandeh@buffalo.edu, Phone: +1-716-645-1523

Health Monitoring of Structural and Biological Systems 2012, edited by Tribikram Kundu, Proc. of SPIE Vol. 8348, 834804 · © 2012 SPIE · CCC code: 0277-786X/12/$18 · doi: 10.1117/12.914848

uncertainty in TOF measurements). As a result of mentioned uncertainties the AE location, TOF and wave velocity are random variables and the procedure of AE source localization can be treated as a probabilistic estimation problem[8].

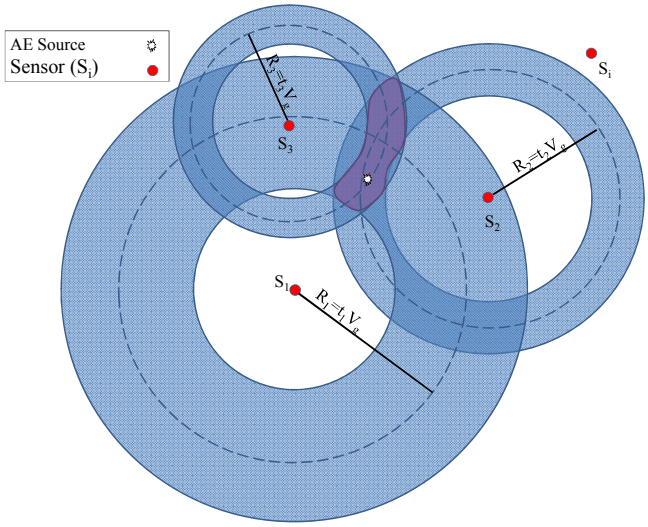

Figure 1. Trilateration with and without noise in distance R_i or equally arrival time t_i and/or V_g.

Several approaches have been proposed in literature for damage/impact localization in plate-like structures. Kundu et al.[4] proposed a method based on optimizing an objective function to find the impact location in isotropic and anisotropic plate. However, the proposed objective function in that reference had the inherent problem of multiple singularities which was overcome in Kundu et al.[12] by modifying the objective function. The optimization technique was further improved by Hajzargarbashi et al.[13]. In references[14,15] the nonlinear least square optimization adopting the Gauss-Newton method was proposed to determine the location, time lag, and velocity of "synthetic" AE signals. Ciampa and Meo[7] used a Newton's iterative method to calculate the coordinates of the impact location and the wave velocity. A Genetic Algorithm (GA) for optimization of an objective function based on the modified triangulation methodology was proposed in reference[16]. We have previously proposed a reliable probabilistic framework in source localization based on Extended Kalman Filter (EKF) estimation[8]. Although the approach improved the accuracy and ability of flexible sensor fusion for location estimation by using EKF, it just considered the systematic error in TOF measurement due to Heisenberg uncertainty in wavelet method utilized for TOF measurement. And we did not take into account the environmental noise effect. Furthermore, implementation of Continues Wavelet Transformation (CWT) in the signal processing stage of the algorithm makes it less practical for real time SHM applications, since continues wavelet is in general computationally expensive. Here we extend our work to improve the efficiency of the algorithm and consider the environmental noise as a source of TOF measurement uncertainty. The paper begins by briefly introducing the TOF based algorithm for the AE source location. Section 3 develops a statistical method based on modeled Lamb waves that are artificially corrupted by noise to correlate noise level to TOF uncertainty. This is followed by section 4 which briefly introduces the EKF theory and its derivation for AE source localization. Section 5 reports the experimental set-up followed by the results in Section 6. Finally, the conclusions are given in section 7.

2. SOURCE LOCATION

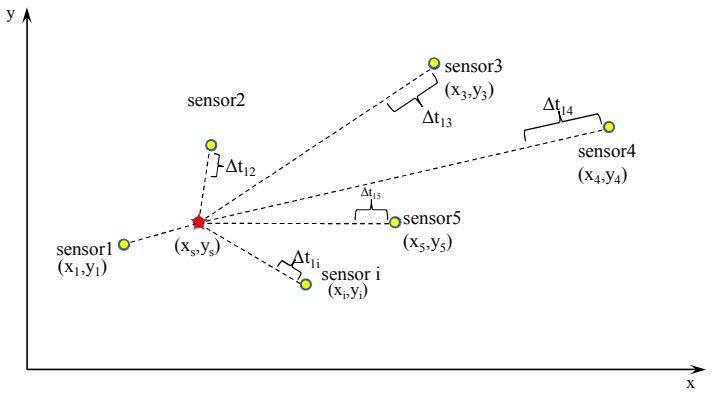

Figure 2. Acoustic emission source and sensors distribution.

Assuming an arbitrary Cartesian coordinate system, the AE source is at unknown coordinates (x_s, y_s) in the plane of the plate and the sensors are located at (x_i, y_i), as shown in figure 2. It is well known that given the wave velocity of a particular Lamb wave mode, at least three sensors are necessary to locate an AE source in plate-like structures. If t_m is the travel time or TOF to reach the first sensor (master sensor), and Δt_{mi} are the time difference between master sensor and the ith sensor, the following equations can be obtained:

$$(x_\mathrm{m} - x_\mathrm{s})^2 + (y_\mathrm{m} - y_\mathrm{s})^2 - \left(t_\mathrm{m} V_\mathrm{g}\right)^2 = 0 \tag{1}$$

$$(x_i - x_\mathrm{s})^2 + (y_i - y_\mathrm{s})^2 - \left[(t_\mathrm{m} + \Delta t_{\mathrm{m}i}) V_\mathrm{g}\right]^2 = 0 \tag{2}$$

where V_g is the group velocity of the particular Lamb wave mode, which is a function of the product of the frequency f and the plate thickness d:

$$V_\mathrm{g} = F(fd) \tag{3}$$

Knowing the properties of the plate, mass density ρ, thickness d, Young's modulus E, and Poisson ratio ν, V_g can be calculated by the *Rayleigh-Lamb equations*[17]. Combining equations (1) and (2) the following equation can be derived:

$$\Delta t_{\mathrm{m}i} = \frac{\sqrt{(x_i - x_\mathrm{s})^2 + (y_i - y_\mathrm{s})^2} - \sqrt{(x_\mathrm{m} - x_\mathrm{s})^2 + (y_\mathrm{m} - y_\mathrm{s})^2}}{V_\mathrm{g}} \tag{4}$$

In general, the difference between the time of flight of master sensor to different sensors (Δt_{mi}) are used to solve this set of nonlinear equations with unknowns $\mathbf{X}=(x_s, y_s, V_g)$. However, as mentioned in the previous section, several sources of error in the time of flight measurements (i.e. dispersion, noise, temperature, etc.), can affect the accuracy of this solution. In this work, to take into account the uncertainties in arrival time t_i or TOF and the wave velocity V_g,, the arrival time t_i and the unknowns x_s, y_s, V_g are treated as mutually independent Gaussian random variables. Based on this assumption, the probability density function of the time difference Δt_{mi} can be also defined as a Gaussian random variable [18] with mean and variance defined as:

$$\Delta t_{\mathrm{m}i} = t_i - t_\mathrm{m}\,, \quad \sigma^2_{\Delta t_{\mathrm{m}i}} = \sigma^2_{t_i} + \sigma^2_{t_m} \tag{5}$$

The determination of time differences Δt_{mi} and the related uncertainties in a noisy environment shall be discussed in section 3. In this probabilistic framework, an Extended Kalman Filter (EKF) approach is used for the optimal estimation of the state vector $\boldsymbol{X} = (x_\mathrm{s}, y_\mathrm{s}, V_\mathrm{g})$.

3. STATISTICAL CHARACTERIZATION OF TOF MEASURMENT

The accuracy of TOF measurement strongly depends on the SNR. In fact, the higher the SNR the lower is the uncertainty in TOF measurement. This section carries out a statistical characterization of TOF errors for a small ambient noise level. At this aims, first flexural Lamb waves are modeled analytically in order to predict the acoustic field in an isotropic plate-like structure generated by an assumed AE source. Then, the simulated signals are corrupted artificially with the noise level using a Monte Carlo simulation in which the statistical distribution of the TOF error is calculated.

3.1 A0 Lamb wave model as a result of continues point excitation

In plate-like structures two fundamental Lamb wave modes can propagate: Symmetric (S_n) and Antisymmetric (A_n). Displacements of the symmetric modes occur in the direction of wave propagation (i.e. extensional modes), whilst antisymmetric modes have displacements transverse to wave propagation direction (i.e. flexural modes). In this paper, it is assumed that only the lowest order flexural mode (A0) is the dominant mode. This is a commonly used assumption, considering that pencil lead breaks on the surface of thin plate, which have been used during the experimental tests to validate the proposed algorithm, predominantly generate the A0 Lamb wave mode[19]. Lamb waves have been modeled by the Ditri's technique with normal point excitation on the surface of plate[20]. In particular, to model the total surface displacements u_z associated with an input of finite duration $f(t)$, a Fourier Transform is used to decompose the input signal into its different frequency components, $f(\omega)$.The input, for pencil lead break simulations, can be assumed as a one cycle toneburst with hanning window and center frequency of 1 MHz[21]. The out of plane displacement as a function of time and distance from the source is given by[20]:

$$u_z(r,t) = \int f(\omega) \sum_m E_m(\omega) H_0^1(k_m r) \exp(-i\omega t)\, d\omega \tag{6}$$

where t is the time, r is the distance from the point source, k_m is wave number of the excited Lamb mode m corresponding to ω, which can be calculated through the phase velocity V_{ph}^m ($k_m = \omega / V_{ph}^m$), and i is imaginary unit; $E_m(\omega)$ is the excitability function for circular crested waves which depend on the angular frequency ω and excited mode m. The spatial variation in crested circular Lamb wave model is expressed by the Hankel function of first kind H_0^1. Using the method of Viktorov[22] the excitability can be computed. The excitability of a mode is totally governed by the amount of out of plane displacement of the mode due to normal point excitation. To model the Lamb wave due to preassumed excitation the A0 mode is considered as the dominant mode and the effect of all other Lamb modes are neglected. Although the assumption of neglecting the effect of other modes is not strictly true, it is almost reasonable since most of excitability for normal point excitation and normal displacement field is strongly related to A0[23]. The phase velocity V_{ph} for different modes and excitability $E(\omega)$ just for fundamental antisymmetric A0 mode, as a function of frequency-thickness are shown in figures 3 and 4 respectively.

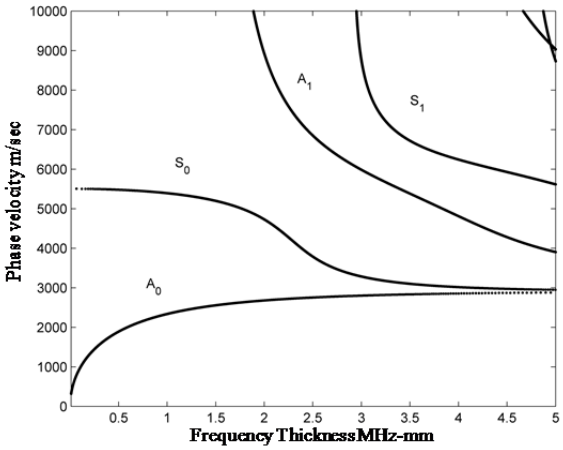

Figure 3. Phase velocity curves for circular crested Lamb waves in aluminum plate.

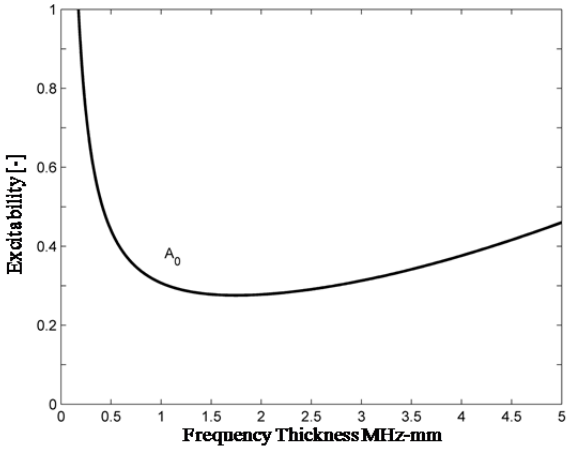

Figure 4. Excitability curves for circular crested Lamb waves in aluminum plate.

The equation (6) enables the surface displacement to be plotted as function of both distance and time, when the plate is excited by a finite duration input at a point. It is assumed that at a sensor position, r, the variation of out of plane displacement u_z with time is directly proportional to output voltage of the sensor. Figure 5 shows some of the modeled signals at different distances to the source. The signals are modeled at range of 5 cm to 50 cm and the duration and sampling frequency of all signals is fixed to 0.2 msec and 3 MHz respectively. All the signals are normalized to the maximum response at 5 cm.

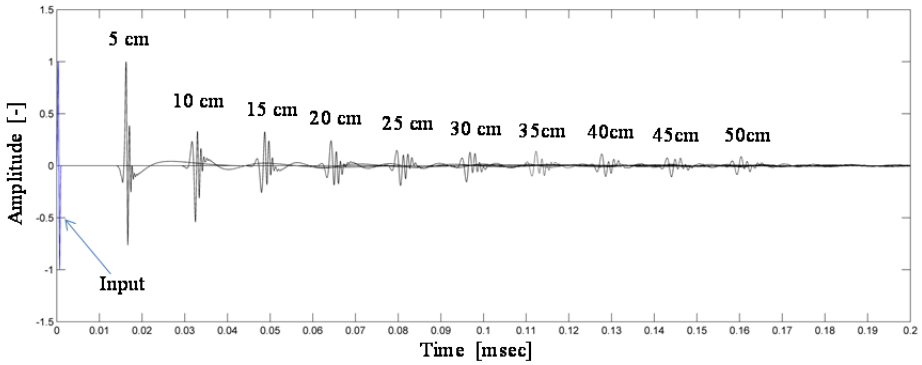

Figure 5. Signal simulation for one cycle sin input in one point with center frequency 1 MHz.

3.2 TOF measurement

Several methods have been proposed in literature for the TOF measurement of acoustic signals, including threshold crossing, coloration methods, wavelet transform, and curve fitting approaches[24]. In this work the TOF has been estimated from both experimental and numerical signal using the maximum envelope method[16]. The envelope can be calculated using the definition of analytic signal $x_A(t)$ of a real signal $x(t)$:

$$x_A(t) = x(t) + ix_H(t) \tag{7}$$

Where i is the imaginary unit and $x_H(t)$ is the Hilbert transformation of $x(t)$defined as:

$$x_H(t) = \frac{1}{\pi}\int_{-\infty}^{+\infty} x(\tau)\frac{1}{t-\tau}d\tau \tag{8}$$

The magnitude of the analytical signal which is identical to the magnitude of the real signal is called envelope:

$$\mathrm{A(t)} = \sqrt{\mathrm{x(t)^2 + x_H(t)^2}} \tag{9}$$

The time instant in which the envelope of the signal reaches its maximum (A_{max}), is considered as the TOF. Envelopes of some of the modeled signals are depicted in figure 6; also the nominal TOF of the simulated signals for distance of 5, 10, and 15 cm are shown in figure 6.

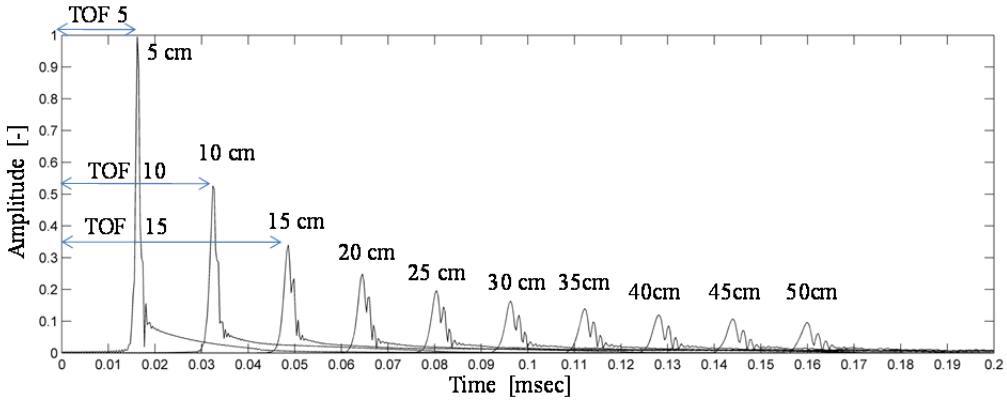

Figure 6. Nominal TOF for different distances.

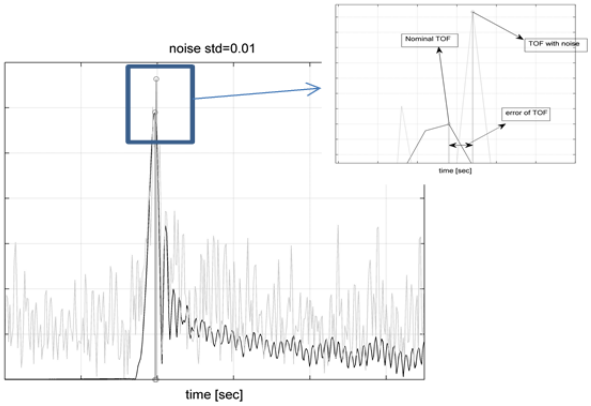

Figure 7. TOF error definition.

3.3 TOF error of noisy data

Investigations on error in TOF measurement of signals due to random noise have been reported for threshold crossing[25], cross correlation[24,26] and some other TOF measurement methods. In this paper the noise modeled as an additive zero mean Gaussian random noise with 0.01standard deviation approximated in the laboratory by means of acquiring several signals in 5 cm distance with several pencil lead breaks as AE sources and normalizing the standard deviation of noise to the average of maximum signal envelopes. It should be noted that the level of the background noise is measured using Root Mean Square (RMS) value of a predetermined portion of signal before the first arrival. In this section the TOF error is defined as the deference between nominal TOF captured from modeled signals and TOF extracted from the

modeled signals artificially contaminated with the noise. For the sake of clarity figure 7 shows a modeled signal at 50 cm from the source with and without noise and the corresponding TOF. This figure simply shows a one simulation of Monte Carlo for a modeled signal at 50 cm and noise level of 0.01.

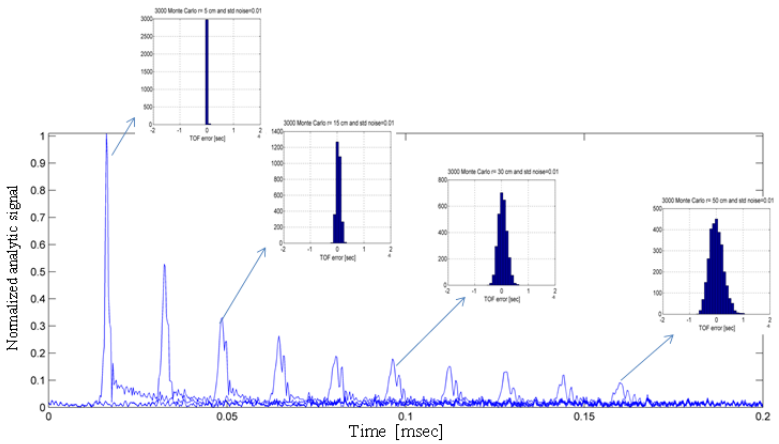

Figure 8. Monte Carlo analysis.

To capture the distribution of TOF error and the corresponding statistics, 3000 Monte Carlo simulations were generated using the noise level and modeled signals at different distances. From the histograms at the top of the figure 8, it can be inferred that as SNR decreases the standard deviation of TOF error (σ_t) increases. The results agree with the expectation of increasing the TOF uncertainty with respect to distance (decreasing SNR). Figure 9 shows the linear relationship between standard deviation of TOF error versus distance to the AE source location.

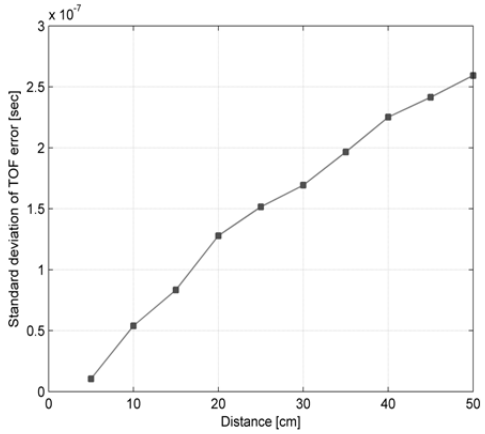

Figure 9. Standard deviation of TOF error versos distance for 0.01 Gaussian random noise and 3000 Monte Carlo analysis.

4. EXTENDED KALMAN FILTER (EKF)

In general, a Kalman Filter (KF) is a recursive data processing algorithm that estimates the *state* of a noisy dynamic system[27]. When we talk about the *state* of a system we mean a vector $\boldsymbol{X}$ consisting of n variables describing some interesting properties of the system. To estimate the state a KF processes all available measurements, both accurate and inaccurate measurements. The KF has been widely used in a wide range of applications due to its simplicity, optimality,

robustness, sensor fusion ability and its capability of filtering out the uncertainties due to the mathematical model and measurements[27,28,29,30]. In general the KF is a two steps process: 1) *state prediction* according to a mathematical model and 2) *correction of the state* according to the measurements collected by sensors. More specifically, in the prediction step the KF estimates the state of the system at a given time instant and then obtains a feedback control in the correction step, by incorporating a new measurement result into *a priori* estimate, in order to gain an improved *a posteriori* estimate. Although the underlying approach is very promising there is a critical limitation. In fact the KF assumes that system and measurements are adequately modeled by a linear dynamic system. The Extended Kalman Filter (EKF) is similar to the KF but it can be used in non-linear systems while making use of first-order Taylor series expansion around the estimated mean[27]. For this reason the EKF has been used to handle the set of nonlinear equations (4).

In this work, the *state* of the system $\boldsymbol{X}$ consists of three parameters, the AE source location (x_s, y_s) and the wave velocity V_g. Given a sparse array of N sensors, the time differences Δt_{mi} between the ith sensor and the master sensor represent the measurement data vector $\boldsymbol{Z} = [\Delta t_{\mathrm{m}i}]_{(N-1)\times 1}$, $N \geq 4$. The *state* of the system $\boldsymbol{X}$ is related to the measurement vector $\boldsymbol{Z}$ through the nonlinear measurement function h defined in equation (4). The key idea underlying the proposed approach is that, the AE source location can be considered as unmovable (static) or slowly fluctuating point. Dehghan Niri and Salamone[8] here simplified the EKF algorithm for AE source localization as follows:

$$\widehat{\boldsymbol{Z}}_{\boldsymbol{k}} = h(\widehat{\boldsymbol{X}}_{\boldsymbol{k-1}}) \tag{10}$$

$\widehat{\boldsymbol{Z}}_{\boldsymbol{k}}$ is predicted measurement vector in kth step according to state estimation $\widehat{\boldsymbol{X}}_{\boldsymbol{k-1}}$ in (k-1)th step using nonlinear measurement function h(.) defined in equation 4.

$$\widehat{\boldsymbol{X}}_k = \widehat{\boldsymbol{X}}_{k-1} + \overline{\boldsymbol{K}}_k(\boldsymbol{Z} - \widehat{\boldsymbol{Z}}_k) \tag{11}$$

Where $\widehat{\boldsymbol{X}}_k$ is estimated states in kth step derived by means of correcting estimated states at (k-1)th step according to difference between actual measurement $\boldsymbol{Z}$ and predicted measurement vector $\widehat{\boldsymbol{Z}}_k$ and Kalman gain $\overline{\boldsymbol{K}}_k$.

$$\widehat{\boldsymbol{P}}_k = (\boldsymbol{I} - \overline{\boldsymbol{K}}_k\boldsymbol{H}_k)\widehat{\boldsymbol{P}}_{k-1} \tag{12}$$

Where $\widehat{\boldsymbol{P}}_k$ is error covariance matrix in kth step.

$$\boldsymbol{H}_k = \left.\frac{\partial h(\boldsymbol{X})}{\partial \boldsymbol{X}}\right|_{\boldsymbol{X}=\widehat{\boldsymbol{X}}_{k-1}} \tag{13}$$

The Jacobian matrix $\boldsymbol{H}_k$ contains the partial derivatives of the measurement function h with respect to the state $\boldsymbol{X}$.

$$\overline{\boldsymbol{K}}_k = \widehat{\boldsymbol{P}}_{k-1}\boldsymbol{H}_k^T\left(\boldsymbol{H}_k\widehat{\boldsymbol{P}}_{k-1}\boldsymbol{H}_k^T + \boldsymbol{R}\right)^{-1} \tag{14}$$

$\overline{\boldsymbol{K}}_k$(3×(N-1) matrix) is the Kalman gain used in correction step.

The objective is to estimate the state vector $\boldsymbol{X} = [x_s, y_s, V_g]$ given the measurement vector $\boldsymbol{Z}$ and covariance matrix $\boldsymbol{R}$. It should be noted that the measurement vector $\boldsymbol{Z}$ in equation (11) does not have the subscript k because its (N-1) components (difference in arrival times) can be considered constant, once the AE signals have been acquired. The uncertainty of measurement vector $\boldsymbol{Z}$ is modeled as a zero mean white Gaussian noise with covariance matrix $\boldsymbol{R}$ with diagonal terms defined in equation (5).

$$\boldsymbol{R} = \begin{bmatrix} \sigma^2_{\Delta t_{\mathrm{m1}}} & \cdots & 0 \\ \vdots & \ddots & \vdots \\ 0 & \cdots & \sigma^2_{\Delta t_{\mathrm{m}(n-1)}} \end{bmatrix} \tag{15}$$

The σ_{ti} has been defined according to distance and fixed level of noise (0.01) in section 3.3. Because the location of the source is certainly unknown parameter the standard deviation can be selected from the average distance of sensors [28.9 cm] and then after estimating the location in each step, the $\boldsymbol{R}$ can be modified iteratively. But as a result of low level of noise and relatively short distance between sensors the assumption of fixed value for standard deviation of TOF error corresponding to average distance is not unreasonable. The standard deviation of TOF error for 28.9 cm and 0.01 noise level according to figure 9 is $1.7 \times 10^{-7} sec$. So from equation (5) $\sigma^2_{\Delta t_{\mathrm{m}i}} = 5.78 \times 10^{-14}\mathrm{sec}^2$.

The EKF will iteratively correct *a priori* knowledge of the state vector $\widehat{\boldsymbol{X}}$and covariance matrix $\widehat{\boldsymbol{P}}$, with respect to the $\boldsymbol{Z}$ and $\boldsymbol{R}$. The iteration begins with the initialization of the state vector estimate $\widehat{\boldsymbol{X}}_0$ and its covariance matrix $\widehat{\boldsymbol{P}}_0$:

$$\widehat{\boldsymbol{X}}_0 = [\hat{x}_{\mathrm{s}_0}, \hat{y}_{\mathrm{s}_0}, \hat{V}_{\mathrm{g}_0}] \tag{16}$$
$$\widehat{\boldsymbol{P}}_0 = \begin{bmatrix} \sigma^2_{\mathrm{x}_{\mathrm{s}0}} & 0 & 0 \\ 0 & \sigma^2_{\mathrm{y}_{\mathrm{s}0}} & 0 \\ 0 & 0 & \sigma^2_{\mathrm{V}_{\mathrm{g}0}} \end{bmatrix}$$

4.1 Initiation of Location

The initial location in x and y direction are modeled as an uncorrelated joint Gaussian probability density function. The upper and lower bound for each coordinate (for example maximum and minimum coordinates of sensors in x and y direction) are computed to calculate the mean and variance of initial location. Then with uniform assumption mean and variance can be expressed as:

$$\hat{x}_{\mathrm{s}_0} = \frac{(x_{\mathrm{sU}} + x_{\mathrm{sL}})}{2} \tag{17}$$
$$\hat{y}_{\mathrm{s}_0} = \frac{(y_{\mathrm{su}} + y_{\mathrm{sl}})}{2}$$

$$\sigma^2_{\mathrm{x_s}} = \frac{1}{12}(x_{\mathrm{su}} - x_{\mathrm{sl}})^2 \tag{18}$$
$$\sigma^2_{\mathrm{y_s}} = \frac{1}{12}(y_{\mathrm{su}} - y_{\mathrm{sl}})^2$$

Having these means and variances the uncorrelated joint Gaussian probability density function of initial location is approximated. Two examples of this joint Gaussian probability density function of initial location are illustrated in figure 10 and their parameters are listed in Table 1. It should be mentioned that by putting the reference of the Cartesian coordinate system on sensor 1 the lower bound for x and y coordinate are zero.

Table 1. Two initial location properties

Initial Gaussian location	1	2
x_{sU}[cm]	12.7	25.4
y_{sU}[cm]	12.7	25.4
$\sigma^2_{\mathrm{x_s}}$ [cm^2]	13.44	53.76
$\sigma^2_{\mathrm{y_s}}$ [cm^2]	13.44	53.76
$\hat{x}_{\mathrm{s}_0}$ [cm]	6.35	12.7
$\hat{y}_{\mathrm{s}_0}$ [cm]	6.35	12.7

It is noteworthy that this approach is robust against the accuracy of initial guess and its sensitivity will be decreased by using the information gathered from more sensors[8].

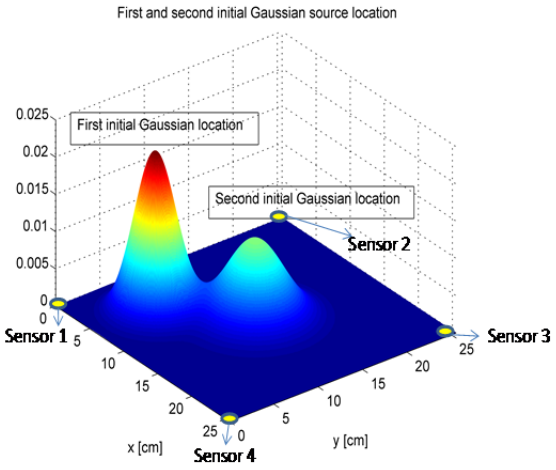

Figure 10. Two different joint Gaussian initial location guesses.

4.2 wave velocity initiation

As a result of dispersive behavior of Lamb wave, the uncertainty in frequency corresponding to measured TOF, directly causes the uncertainty in group wave velocity assumption even with knowledge of dominant Lamb mode (here A0). In this research, we propose to assume that the maximum of Fourier transformation of each acquired signal corresponds to its TOF measured by means of maximum envelope approach. It should be insisted that this assumption is not strictly accurate since the Lamb wave signals can be totally nonstationary. However, with probabilistic consideration of V_g and considering it as one of the estimation parameters in this method, its true value will be estimated. If F_i represents the maximum of Fourier transformation of ith recorded signal its velocity V_{gi} can be defined form group A0 Lamb wave dispersion equation (4) as:

$$V_{\mathrm{gi}} = F(F_i d) \tag{19}$$

The mean of V_{gi} or initial group wave velocity $\hat{V}_{g_0}$ is calculated as:

$$\hat{V}_{g_0} = \bar{V}_g = \frac{\sum_1^N V_{g_i}}{N} \tag{20}$$

And its variance $\sigma_{V_g}^2$ easily can be calculated as:

$$\sigma_{V_g}^2 = \frac{\sum_1^N \left(V_{g_i} - \bar{V}_g\right)^2}{N} \tag{21}$$

Examples of this Gaussian probability of V_g are illustrated in figures 13 d).

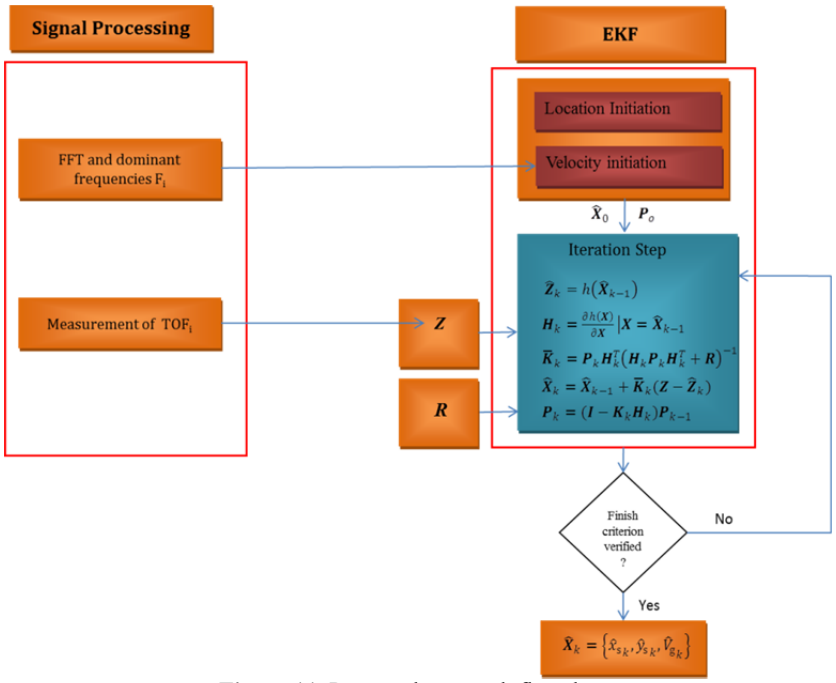

Figure 11. Proposed approach flowchart.

Overall, the proposed approach consists of two stages as shown in the flowchart in figure 11; the first stage provides information about time of arrivals, frequency and their uncertainties; the second stage uses *a priori* information about the states and iteratively estimate the state vector according to the measured information obtained from the first stage.

5. EXPERIMENTAL SETUP

Experiments were carried out using an aluminum plate with dimensions 910mm×910mm×3.175mm to validate the proposed algorithm. The plate was instrumented with an array of four piezoelectric transducers in a square configuration, with 254 mm dimension. The experimental set-up is shown in figure 12. For the data acquisition, a LeCroy Wave runner oscilloscope with sampling frequency of 3 MHz was used. Each sensor was connected to a preamplifier. During testing, AE sources were generated by pencil lead breaks at 4 systematic grid locations. Post-processing of the received signals was performed with a PC running a Matlab software code implemented by the authors. The number of iteration in EKF stage is fixed to 15.

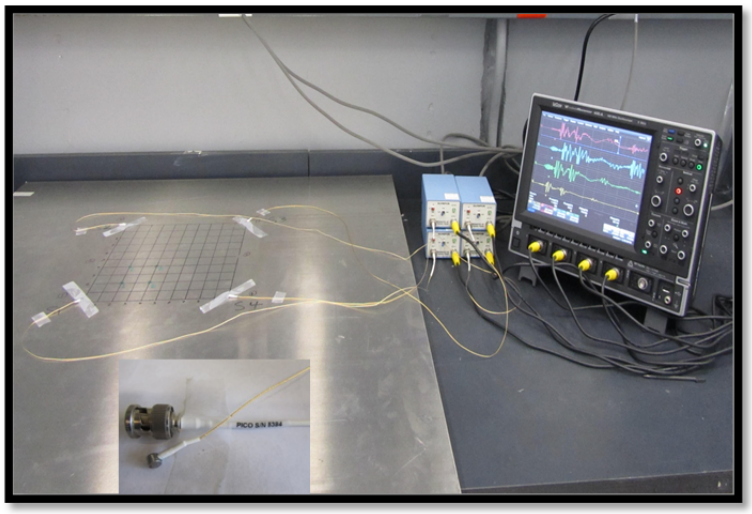

Figure 12. Experimental set up.

6. RESULTS AND DISCUSSION

Four AE source were simulated using pencil lead break and the proposed procedure was applied. Figure 13 shows the signal processing and velocity initiation part of the procedure for point #1 illustrated in figure 14. The results prove the validity of the proposed method in fast and accurate location estimation of AE sources. Table 2 listed the actual and average estimated position of each source using first and second initial location guesses shown in figure 10. Result of 2.3 mm error in average in x and y coordinates demonstrates the high accuracy gained with this versatile method. The number of iteration to reach these results is 7. Figure 14 depicts actual and estimated source locations. Computational time on regular personal computer for each source location using the proposed algorithm took less than 0.03 sec, showing this algorithm is appropriate for real-time AE applications using compiled code.

The results show a slight improvement in accuracy compared to the results achieved in the previous work[8]. Although the signal processing stage used to extract time-frequency information in this paper is more sensitive to random noise than CWT utilized in the previous investigation[8], it is significantly more efficient than the CWT.

Table 2. Actual and estimated source positions and estimated wave velocity. (with the first initial location)

Point no:	1	2	3	4
x_{s_a}(mm)	50.8	101.6	50.8	101.6
$\hat{x}_s$ (mm)	51.73	103.4	50.9	105.2
y_{s_a}(mm)	50.8	50.8	101.6	101.6
$\hat{y}_s$(mm)	51.99	58.47	102.0	104.3
$\hat{V}_g(m/sec)$	3149	2998	2891	2728
The origin of Cartesian coordinates is at sensor 1				

Using two different initial location guesses which are almost far from each point demonstrates that the fast convergence of EKF is highly insensitive to initial guesses unlike other optimization methods like simplex, and Newton.

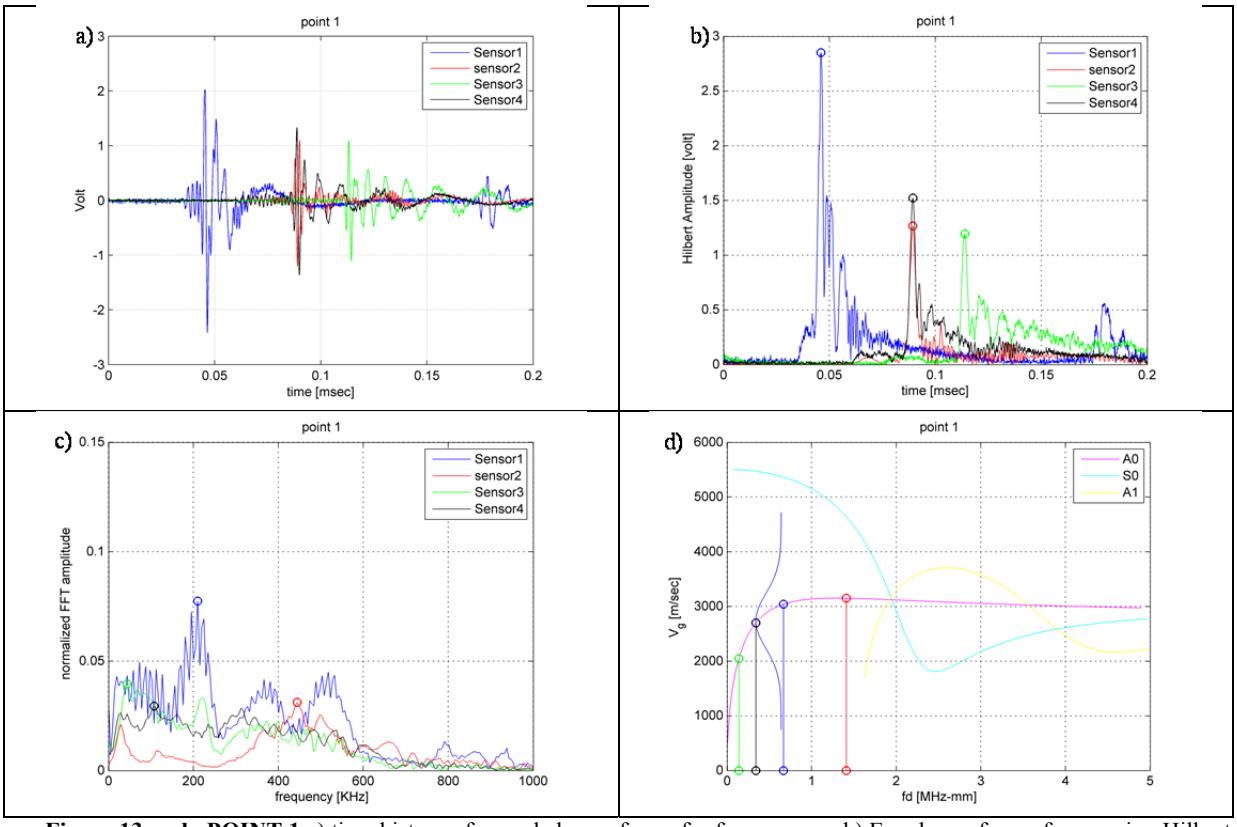

Figure 13. a-d, POINT 1 a) time history of recorded waveforms for four sensors. b) Envelope of waveforms using Hilbert transformation. c) FFT of recorded signals d) Initiation of group wave velocity of A0 Lamb mode.

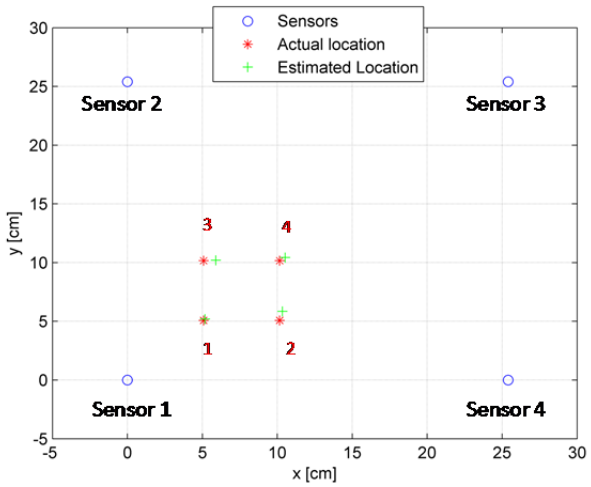

Figure 14. Impact location estimation results for four points.

7. CONCLUSION

In this paper a probabilistic framework for locating acoustic emission sources is proposed based on the EKF theory. The proposed approach, in which TOF and wave velocity are considered as Gaussian random variables, consists of two main

stages. In the first stage TOF measurement of Lamb waves are carried out by maximum envelope approach and providing the probabilistic information of group wave velocity of A0 Lamb mode based on FFT of signals and A0 group velocity depression curve. Random portion of TOF uncertainty as a result of fixed level of noise are considered and modeled numerically by means of modeling signals as a result of predefined normal point excitation and using excitability function of A0 mode for normal displacement field. The second stage EKF uses the information extracted from the first stage and iteratively estimates AE location and wave velocity. In addition to advantages that reported in reference[8] like the capability of: (1) taking into account uncertainties in TOF measurements and wave velocity and (2) efficiently fuse multi-sensor data to perform an efficient AE source localization, by using more efficient signal processing stage in this paper the algorithm becomes more appealing for on-line structural health monitoring. The performance of the proposed algorithm has been validated through pencil-lead breaks performed on an aluminum plate at systematic grid locations. The plate was instrumented with an array of four piezoelectric transducers.

REFERENCES

[1] Staszewski, W., Boller, C., Tomlinson, G., [Health Monitoring of Aerospace Structures Smart Sensor Technologies and Signal Processing], JOHN WILEY & SONS, (2004).

[2] Giurgiutiu, V. and Bao, J., "Embedded-ultrasonics structural radar for in situ structural health monitoring of thin-wall structures", Struct. Health Monit.: Int. J. 3, 121-140 (2004).

[3] Su, Z. and Ye, L. "Fundamental Lamb mode-based delamination detection for CF/EP Composite laminates using distributed piezoelectrics", Struct. Health Monit.: Int. 3, 43-68(2004).

[4] Kundu, T., Das, S. and Jata, K. V., "Point of impact prediction in isotropic and anisotropic plates from the acoustic emission data", J. Acoust. Soc. Am. 122, 2057-2066(2007).

[5] Kundu, T., Das, S., Martin, S. A. and Jata, K. V., "Locating point of impact in anisotropic fiber reinforced composite plates" Ultrasonics 48, 193-201(2008).

[6] Salamone, S., Bartoli, I., Leo, P. D., Scalea, F. L. D., Ajovalasit, A., Acquisto, L. D., Rhymer, J. and Kim, H., "High-velocity Impact Location on Aircraft Panels Using Macro-fiber Composite Piezoelectric Rosettes", J. Intell. Mater. Syst. Struct., 21, 887-896(2010).

[7] Ciampa, F. and Meo, M. "Acoustic emission source localization and velocity determination of the fundamental mode A0 using wavelet analysis and a Newton-based optimization technique", Smart Mater. Struct., 19, 045027 (2010).

[8] Dehghan Niri, E. and Salamone, S., "A Probabilistic Framework for Acoustic Emission (AE) Source Localization in Plate-Like Structures", Smart Mater. Struct., accepted Jan (2012).

[9] Salamone, S., Bartoli, I., Lanza, di., Scalea, F. and Coccia, S., "Guided-wave Health Monitoring of Aircraft Composite Panels under Changing Temperature", J. Intell. Mater.Syst.Struct., 20, 1079-1090(2009).

[10] Haywood, J., Coverley, P. T., Staszewski, W. and Worden, K., "An automatic impact monitor for a composite panel employing smart sensor technology", Smart Mater. Struct., 14, 265-271(2005).

[11] Leclerc, J., Worden, K., Staszewski, W. and Haywood, J., "Impact detection in an aircraft composite panel—A neural-network approach", J. Sound Vib., 299, 672-82(2007).

[12] Kundu, T., Das, S. and Jata, K. V., "Detection of the point of impact on a stiffened plate by the acoustic emission technique", Smart Mater. Struct., 18, 035006(2009).

[13] Hajzargerbashi, T., Kundu, T., and Bland, S., "An improved algorithm for detecting point of impact in anisotropic inhomogeneous plates", Ultrasonics, 51, 317-324(2011).

[14] Gaul, L., "Identification of the impact location on a plate using wavelets", Mechanical Systems and Signal Processing, 12, 783-795(1998).

[15] Gaul, L., Hurlebaus, S., and Jacobs, L., "Localization of a synthetic acoustic emission source on the surface of a fatigue specimen", Res. Nondestruct. Eval., 13, 105–117(2001).

[16] Coverley, P. T., and Staszewski, W., "Impact damage location in composite structures using optimized sensor triangulation procedure", Smart Mater. Struct., 12, 795-803(2003).
[17] Auld, B. A., [Acoustic Fields and Waves in Solids], JOHN WILEY & SONS, (1973).
[18] Soong, T. T. [Fundamentals of Probability and Statistics for Engineers], JOHN WILEY & SONS,(2004).
[19] Gorman, M. R. and Prosser, W. H., "AE source orientation by plate wave analysis", J.Acoust. Emiss. 9, 283-288(1991).
[20] Wilcox, P. D.,"Lamb wave inspection of large structures using permanently attached transducers", Thesis of PhD degree, Department of Mechanical Engineering, Imperial College of Science, Technology and Medicine London, SW7 2BX, (1998).
[21] Banerjee, S. , Mal, A. K., and Prosser, W. H., "Analysis of transient Lamb waves generated by dynamic surface sources in thin composite plates" J. Acoust. Soc. Am., 115, 1905-1911 (2004).
[22] Viktorov, I. A., [Rayleigh and Lamb Waves: Physical Theory and Applications], New York: Plenum Press, (1967).
[23] Wilcox, P.D., Cawley, P., Lowe, M. J. S., , "Acoustic fields from PVDF interdigital transducers" Science, Measurement and Technology, Proc. IEEE, 145, 250-259 (1998).
[24] van der Heijden, F., Duin, R.P.W. , de Ridder, D., and Tax, D. M. J., [Classification, Parameter Estimation, and State Estimation], JOHN WILEY & SONS, (2004).
[25] Andria, G., "Digital signal processing techniques for accurate ultrasonic sensor measurement", Measurement, 30, 105-114 (2001).
[26] Parrilla, M. , Anaya, J. J., and Fritsch, C. , "Digital signal processing techniques for high accuracy ultrasonic range measurements", IEEE Transactions on Instrumentation and Measurement,40,759-763(1991).
[27] Crassidis, J. L., and Junkins, J. L., [Optimal Estimation of Dynamic Systems], Chapman & Hall/CRC Applied Mathematics & Non-linear Science, Boca Raton,(2004).
[28] Sabatini, A. M., "A digital signal-processing technique for compensating ultrasonic sensors", IEEE Trans. Instrum. Measur., 44, 869-874(1995).
[29] Tsai, C. C., "A localization system of a mobile robot by fusing dead-reckoning and ultrasonic measurements", IEEE Trans. Instrum. Measur. 47, 1399-1404(1998).
[30] Moreno, V. M., and Pigazo, A., [Kalman Filter: Recent Advances and Applications], InTech, (2009).